# Hemolytic Iron Regulation in Traumatic Brain Injury and Alcohol Use

**Agnieszka Agas** ( ama59@njit.edu )
New Jersey Institute of Technology https://orcid.org/0000-0001-8564-3168
**Arun Reddy Ravula**
New Jersey Institute of Technology
**Xiaotang Ma**
New Jersey Institute of Technology
**Yiming Cheng**
New Jersey Institute of Technology
**Kevin D. Belfield**
New Jersey Institute of Technology
**James Haorah**
New Jersey Institute of Technology

**Research Article**

**Keywords:** alcohol, TBI, hemorrhage, iron, microglia

**Posted Date:** April 7th, 2022

**DOI:** https://doi.org/10.21203/rs.3.rs-991124/v2

# Abstract

Hemorrhage is often a major component of traumatic brain injury (TBI). Red blood cells (RBCs), accumulated at the hemorrhagic site, undergo hemolysis upon energy depletion. Hemolysis of RBCs is expected to release free iron into the central nervous system (CNS) which must be managed to prevent iron neurotoxicity. Here, we examine the hypothesis that chronic alcohol consumption, as a secondary stressor, may increase iron toxicity in a rat model of TBI by altering the iron management pathways. We found large accumulations of free iron at the site of hemorrhage with evidence of hemolytic activity. Our observations demonstrate that alcohol use can alter the three distinct iron management pathways: transferrin/hemosiderin binding, lipocalin 2/heme oxygenase 1/ferritin system, and possible microglial phagocytosis. Presence of alcohol prolonged the expression of lipocalin 2 as well as increased and sustained levels of ferritin, while the combined effects of alcohol and TBI elevated the levels of heme oxygenase 1 faster than TBI alone. The hippocampus, neocortex, ventricles, and around vessels near the site of impact appeared to be the prominent brain regions of induction. In addition, we provide evidence that microglia my also play a role in iron management through RBC phagocytosis.


# Highlights

- Chronic alcohol exposure increases hemorrhage and RBC accumulation following FPI.
- Alcohol alters iron regulatory patterns by shifting LCN2, HO-1, and F-LC expressions.
- Activated microglia may regulate iron accumulation by possibly phagocytosing RBCs.

# 1. Introduction

Traumatic brain injury (TBI) is an acquired form of injury to the brain caused by an external force that results in either mild, moderate, or severe neurological dysfunction. Animal models reproducing different types of TBI, including focal contusions/penetrating injuries with fluid percussion or weight-drop devices and diffuse/non-penetrating injuries with blast tubes or also weight-drop devices, have observed inflammation, edema, oxidative stress, and blood-brain barrier breach following the insult and corresponding to behavioral deficits [1-4]. One of the major pathological events of TBI is intracranial and, subsequently, intracerebral hemorrhaging including epidural, subdural, subarachnoid, and intraventricular hematomas [5, 6]. Such blood suffusions are constantly being detected in TBI patients by fast magnetic resonance imaging and computerized tomography scanning [7].

Alcohol use and TBI are inexplicably linked, with one being a risk factor and modulator of the other [8]. Beyond the cognitive and psychosocial, alcohol use has been shown to prolong neuroinflammation and

neurodegeneration at post-TBI by impairing neurological recovery and exacerbating localized neuroinflammation [9, 10]. In addition, as an antiplatelet and anticoagulant, alcohol can ‘thin’ blood and lead to more profuse bleeding [11]. Therefore, chronic alcohol consumption lengthens bleeding times of injured soft tissue by reducing platelet aggregation. Alcohol can even interact with platelet cyclooxygenase-1 to inhibit its function and prevent subsequent development of pro-aggregatory proteins. Other hemodynamic changes in blood pressure and vessel integrity can also contribute to increased bleeding with alcohol.

In our rat model of blunt TBI, we have observed massive RBC aggregations at the site of hemorrhage [12]. This TBI model uses lateral fluid percussion injury (FPI) delivered at a moderate pressure to reproduce TBI without skull fracturing to generate hemorrhage, subdural hematoma, and edema. FPI causes the rupture of blood vessels through various transient mechanical forces generated by the impact [13]. Even though there are various TBI models, FPI reproducibly recapitulates the pathophysiological signatures of human TBI and thus, can be used to examine the fate of RBCs at post-TBI [13]. In this study, we include alcohol use to our TBI model and focus on examining whether alcohol augments hemorrhage and results in greater and even faster accumulations of RBCs in the central nervous system (CNS).

Brain hemorrhages are observed in conjunction with anemia and coagulopathy, therefore current treatment practices include anticoagulant or red blood cell (RBC) transfusions [14, 15]. Interestingly, these therapies do not improve neurological function, in fact, RBC transfusions have been shown to significantly exacerbate trauma complications [16]. Since RBCs contain much of the iron found in the body, a possible reason for unresolved, persistent cognitive functional deficits may be neurotoxicity caused by an iron overload [17]. As blood vessels rupture and RBCs are removed from the circulation, accumulating RBCs, lacking a mitochondria, begin to undergo lysis upon energy depletion [18]. Hemolysis of RBCs releases iron, carbon monoxide, and biliverdin into the CNS [19]. Destruction of RBCs also involves hemolysis and release of RBC constituents, including hemoglobin, heme, and iron, into the extracellular space. Immediately following injury, this released iron is in a toxic free, ferrous ($Fe^{2+}$) form that, over time, is oxidized to the insoluble ferric ($Fe^{3+}$) species [20].

The hemolytic product iron is managed by several different proteins to prevent possible iron toxicity that may develop from iron accumulation. Chief iron regulators include heme oxygenase-1 (HO-1, iron release), lipocalin 2 (LCN2, intracellular iron transport), ferritin light chain (F-LC, iron storage), transferrin (extracellular iron transport), and hemosiderin (iron storage and sequestration) [21, 22]. Together, these proteins combine to form two distinct pathways for iron management, the LCN2/HO-1/F-LC system for intracellular iron and transferrin/hemosiderin binding for extracellular iron. These pathways have been studied following TBI alone, but, to our knowledge, there has been no examination of iron management under combined alcohol and TBI. As alcohol use is closely associate with TBI, as a secondary stressor, alcohol may affect RBC clearance and iron regulation. In this study, we also examine the fate of these TBI-induced iron regulatory pathways and their time dependent coordination under prior chronic alcohol consumption.

Many studies have already shown that traumatic brain injury activates microglia [23]. Microglia become activated after transitioning through a series of activation states [24]. During this time, microglia undergo changes in both morphology and function. As a result, activated microglia may also play a role in iron management. In a final observation to this study, we also show evidence that microglia may be involved in clearing away dying RBCs and accumulating iron deposits.

# 2. Methods And Materials

*2.1 Reagents*

The OCT compound was purchased from Fisher Healthcare (#4585). Prussian blue soluble was purchased from Santa Cruz (sc-215757), eosin 5% from Sigma (#R03040-74), and hematoxylin solution from Merck (#HX69851575). Primary antibodies were purchased from Santa Cruz, Thermo Fisher, proteintech, and Abcam (**Table 1**). Secondary antibodies were purchased from Thermo Fisher (#32230 and # 32260) for western blots and Abcam (ab64255 and ab97049) for immunohistochemistry. The streptavidin protein was purchased from Abcam (ab7403), Pierce DAB substrate kit from Thermo Fisher (#34002), and Cytoseal XYL from Thermo Scientific (#8312-4). The bicinchoninic acid kit for protein determination was purchased from Thermo Fisher (#23227) and the 4–20% precast protein gel (4561094) and trans-blot PVDF transfer kit (#1704272) were purchased from Bio-Rad. The chemiluminescent substrate was purchased from Advansta (#K-12045-D50). All reagents and antibodies were validated for specificity by the companies.

*2.2 Animals*

Male Sprague-Dawley rats were purchased from Charles River Laboratory (Wilmington, MA), they were approximately 8 weeks old and weighed about 240-270 grams at the beginning of the experiment. Rats were kept in reversed 12 hrs. light/dark cycle and housed in controlled temperature and humidity conditions. Power analysis was conducted prior, and a sample size of N = 4 rats was required for histological analysis (80% power). Adequacy of sample size was determined from previous work. All experiments were conducted in accordance with the National Institutes of Health institutional ethical guidelines for care of laboratory animals and approved by the Institutional Animal Care Use Committee of Rutgers University (Newark, NJ) IACUC Protocol No. PROTO999900801.

*2.3 Alcohol Feeding*

Ethanol liquid-diet pair-feeding was employed according to our previously described procedure [25-27]. Briefly, equal pairs of weight-match rats were acclimated to Lieber-DeCarli control or 29% calorie (5% v/v) ethanol liquid-diets (Dyets Inc., Bethlehem, PA) for 1 week followed by pair feeding regimens for 12-14 weeks. Feeding of the control group was based on the amount of ethanol-liquid diet consumed by

ethanol group. The control-liquid diet was composed of 47% carbohydrate, 35% fat, and 18% protein while the ethanol-liquid diet was composed of 19% carbohydrate, 35% fat, 18% protein, and 29% ethanol as percent of total caloric intake. Daily food intake was monitored, and weekly body weights were recorded. By the end of the experiment, the average body weight was 410-420 grams for the control group and 460-490 grams for the ethanol group. Prior to sacrifice, the blood alcohol concentration of all the rats on the ethanol-liquid diet was measured, and it was found to be 9.1-28.8 mM with an average of 15.6 mM which is consistent with our previous findings [25-27].

### *2.4 Fluid Percussion Injury*

After alcohol feeding, traumatic brain injury was performed using a fluid percussion injury (FPI) model (Amscien Instruments, Richmond, VA) according to our previously described procedure [13, 28]. Briefly, rats were anesthetized with ketamine (100 mg/kg body weight) and xylazine (10 mg/kg body weight) through intraperitoneal injection and positioned on a stereotaxis frame. Craniotomy was performed by drilling a 3.0 mm size hole on the left parietal skull (2.5 mm lateral of the sagittal suture, 3.0 mm caudal of the coronal suture) leaving the dura intact. A Luer Lock hub was glued to the skull over the exposed dura with cyanoacrylate glue and secured with methyl-methacrylate resin (Henry Schein, Melville, NY). The next day, animals were anesthetized by isoflurane and received lateral FPI. Briefly, the Luer Lock hub of the animal was filled with fluid and fitted into the nozzle of the FPI device. Injury was induced by a pendulum weight striking the piston of a fluid filled cylinder and delivering a fluid pressure pulse to the exposed dura. Severity of the injury was controlled by the position of the weight on the pendulum, all animals received moderate injury or around 2.0 atm pressure [13]. After injury, the hub was removed, the head was sutured, and the rat was returned to its cage. Control animals did not undergo surgery, sham animals underwent surgery but did not receive an injury.

### *2.5 Tissue Processing*

Animals were sacrificed at time points between 2 hours to 7-days post-injury. Blood samples were collected from the carotid artery and used in western blot analysis. Brains were removed from the skull and thoroughly washed in PBS. Cryopreservation was performed by subsequent overnight incubations in 4% paraformaldehyde, 10% sucrose, and 30% sucrose, respectively. Brains were then snap-frozen in Tissue-Tek OCT compound (Thermo Fisher, Waltham, MA) and stored at 80$^{o}$C until slicing. Coronal sections (10-20 μm) were cut on a Leica CM3050 cryostat and collected on Fisherbrand Superfrost Plus slides. Slides were air-dried overnight and then stored at -80$^{o}$C until staining.

### *2.6 Prussian Blue*

This reaction detects ferric iron ($Fe^{3+}$) in tissue sections. Treatment with acidic solutions of ferrocyanides causes any ferric ions (+3) in the tissue to combine with ferrocyanide and form blue pigments of ferric ferrocyanide [20]. Sections were fixed in ice cold methanol for 10 mins., dried for 20 mins, and rehydrated in PBS for 10 mins. Sections were incubated in a working solution of 5% potassium ferrocyanide with 5% hydrochloric acid for 30 mins. after which they were thoroughly washed in distilled water before being counterstained with eosin for 1 min. The working solution was prepared fresh every time and discarded after use. Results show iron (hemosiderin) as blue, vessels/red blood cells as bright pink, and tissue as light pink.

*2.7 Turnbull's Blue*

This reaction detects ferrous iron ($Fe^{2+}$) in tissue. The crystalline structures of Prussian blue and Turnbull's blue compounds are identical but the method by which they are formed is different. Treatment with an acidic solution of potassium ferricyanide causes any ferrous ions (+2) in the tissue to react and form blue pigments of ferrous ferricyanide [20]. Sections were fixed in ice cold methanol for 10 mins., dried for 20 mins, and rehydrated in PBS for 10 mins. Sections were incubated in a working solution of 0.4 mg potassium ferrocyanide with 40 mL 0.006 N hydrochloric acid for 1 hr. after which they were thoroughly washed in 1% acetic acid before being counterstained with eosin for 1 min. The working solution was prepared fresh every time and discarded after use. Results show ferrous iron as blue, vessels/red blood cells as bright pink, and tissue as light pink.

*2.8 Immunohistochemistry*

Prussian and Turnbull's blue were combined with immunohistochemistry in a modified technique previously described by Blomster et., al [29]. Following Prussian or Turnbull's blue staining, sections were incubated with 0.3% $H_2O_2$ for 10 mins. to quench any endogenous activity. After washing, slides were permeabilized with buffer containing 1% bovine serum albumin and 0.4% Triton X-100 in phosphate buffered saline (PBS) then incubated with 10% bovine serum albumin and 0.4% Triton X-100 in PBS to block non-specific antibody binding. The sections were incubated overnight in a humidified chamber at 4$^{o}$C with diluted primary antibody: mouse anti-heme oxygenase 1 (1:50, Santa Cruz), rabbit anti-Iba1 (1:200, Abcam), rabbit anti-NGAL (1:500, Thermo Fisher), or rabbit anti-ferritin light chain (1:25, proteintech) (**Table 1**). The following day, slides were thoroughly washed in PBS and incubated with the appropriate secondary antibody, biotinylated goat anti-rabbit (1:500, Abcam) for 1 hr. or biotinylated goat anti-mouse (ready-to-use, Abcam) for 20 mins. After washing, slides were incubated with streptavidin-HRP (1:10,000, Abcam) for 30 mins. After a final washing, staining was developed with 3,3'-diaminobenzidine tetrahydrochloride (DAB, Thermo Fisher) for 20 mins., immersed in distilled water to stop the reaction, and counterstained with eosin for 1 min. Alternatively, slides were counterstained with hematoxylin for 10 mins. and washed in running tap water for 10 mins. Sections were dehydrated

through 4, 2 min. changes of alcohol (95%, 95%, 100%, and 100%) and mounted with Cytoseal XYL (Thermo Fisher) solution. Results show stained protein as brown, iron as blue, red blood cells as bright pink, and tissue as light pink. Images were captured with a Leica DMi1 or Aperio Versa 200 widefield microscope digital pathology scanner at 20x magnification with an image matrix of 1024 × 1024 pixel. Protein expression was semi-quantified in a technique described by Crowe et., al [30, 31]. Briefly, DAB and hematoxylin staining were digitally separated using ImageJ Fiji software and subjected to measurement of mean gray values (DAB) and number of nuclei (hematoxylin). Expression levels of the protein were determined as the average of the gray values normalized by nuclei number.

### *2.9 Western Blotting*

Whole body blood was collected and centrifuged at 2,100 x g for 10 mins. to separate the plasma for analysis. Protein concentration was estimated using the bicinchoninic acid (BCA) method (Thermo Fisher). 20 µg/lane of protein was loaded into the wells of 4–20% precast polyacrylamide gels (Bio-Rad, Hercules, CA) for separation. Separated proteins were transferred onto PVDF membranes, blocked with 5% non-fat milk, and incubated at 4$^{o}$C overnight with the respective antibody (1:1,000 dilution) (**Table 1**). The following day, slides were thoroughly washed in tris-buffered saline with 0.1% Tween 20 and incubated with the appropriate secondary antibody, horse-radish peroxidase conjugated goat anti-mouse or horse-radish peroxidase conjugated goat anti-rabbit for 1 hr. (both 1:10,000, Thermo Fisher). After a final washing, immunoreactive bands were detected with WesternBright ECL chemiluminescent substrate (Advansta) read on a ChemiDoc Imaging System (BioRad Laboratories). Digital images of the bands were produced with Softmax Pro Software (Medical Devices). Data was quantified as arbitrary intensity units with densitometry analysis using Image J software.

### *2.10 Statistical Analysis*

Statistical analysis was performed to determine a significant difference in the amount of protein expression between Sham and EtOH, FPI, or EtOH + FPI. Immunohistochemistry results were analyzed with two-way repeated measures ANOVA with Tukey's multiple comparisons test and western blot results were analyzed with unpaired t tests using GraphPad Prism version 9.0.0 for Windows (GraphPad Software, San Diego, CA). Shapiro-Wilk tests were used to validate that the data was normally distributed and Levene's test to check groups did not significantly deviate from variance. Data are presented as mean ± standard deviation from the mean (SD). The threshold for statistical significance was $p \leq 0.05$ ($* p \leq 0.05$, $** p \leq 0.01$, $*** p \leq 0.001$, and $**** p \leq 0.001$). Authors were blinded to the experimental protocol while performing the experiments, image captures, and statistical calculations.

# 3. Results

*3.1 Iron accumulation is directly proportional to RBC aggregation following TBI.*

Prussian and Turnbull's blue methods were sensitive enough to stain for iron produced by just one RBC (**Fig. 1**, Eosin + Prussian Blue at 7 days panel). In addition, both Prussian and Turnbull's blue were able to penetrate cells and stain for iron present inside intact vessels (**Fig. 1**, Eosin + Prussian Blue at Sham panel). Finally, these methods did not interfere with other chromogens, such as the naturally occurring bilirubin (**Fig. 1**, Prussian Blue at 7 days panel), however the overlay of multiple stains did cause positive iron to appear different shades of dark blue. Large bleeding in the ventricular systems showed presence of ferrous iron 2 hours post-TBI but by 7-days all iron was converted to the ferric form (**Fig. 1**, Turnbull's Blue at 2 hours and Prussian Blue at 7-days panels). Understandably, large bleed sites accumulated large deposits of iron while small sites contained considerably less iron. Therefore, the amount of excess iron aggregation depends on the number of RBCs released at the hemorrhagic sites of TBI.

*3.2 Ethanol exposure alters peak LCN2, HO-1, and F-LC expression TBI.*

*3.2.1 Moderate lateral fluid percussion injury.*

We found that the presence of intracellular iron transporter lipocalin 2 (LCN2) was most notable directly at the site of impact, the expression of LCN2 peaked at 24 hours post-TBI and returned to Sham levels after 3 days post-injury (**Fig. 2**, FPI panels at 1-, 3-, and 7-days). Interestingly, LCN2 was found in individual cells throughout the tissue at 24 hours, most significantly in cells surrounding both ruptured and intact vessels. This early expression post-injury is attributable to LCN2 involvement in the innate immune response. Similarly, increase in the levels of heme oxygenase-1 (HO-1) was observed in the hippocampus and neocortex, prominently around the site of impact. The increase in HO-1 level peaked at day 3 post-injury and it was significantly reduced at day 7 post-injury, which was then found to be localized around the vessels (**Fig. 3**, FPI panels at 1-, 3-, and 7-days).

LCN2 and HO-1 are both stress-responsive proteins, as such both protein levels were expected to significantly increase upon RBC degeneration at day 3 post-injury., Western blot analysis showed that, unlike LCN2, there was significant increase in HO-1 levels ($p<0.001$) compared with sham controls (**Fig. 5**). This discrepancy can be explained by LCN2 being primarily localized to the impact site and HO-1 being much more dispersed. In addition, our western blotting was performed on plasma samples, therefore measuring LCN2 or HO-1 proteins that have leaked into the circulatory system. Unlike LCN2 and HO-1, the localization of the iron storage protein ferritin light chain (F-LC) was more perilesional, found in the hypothalamic and basal forebrain regions of the brain. The increase in clusters of F-LC, ranging from

<1 μm to 50 μm in size, was observed time-dependently (1-7 days) post-injury FPI around the RBCs and iron deposits in these areas (**Fig. 4**, FPI panels at 1-, 3-, and 7-days). This increase in qualitative levels of F-CL ($p<0.001$) compared with sham controls was further validated by quantitative Western blot analysis (**Fig. 5**). These results are in accordance with those reported by Russell et. al. (2019) that also looked at the expression levels of LCN2, HO-1, and F-LC in an FPI model of TBI [22].

*3.2.2 Chronic alcohol consumption and FPI.*

In the CNS, one result of chronic alcohol consumption was increased presence of LCN2 (**Fig. 2**, Sham and EtOH panels at 1-, 3-, and 7-days), HO-1 (**Fig. 3**, Sham and EtOH panels at 1-, 3-, and 7-days), and F-LC (**Fig. 4**, Sham and EtOH panels at 1-, 3-, and 7-days) when compared to the no alcohol control. As a physiological stressor, ethanol can induce expression of these stress-responsive proteins. Expression was generally ubiquitous for all three proteins, however, some areas along the edge of the neocortex, did show greater expression. The magnitude of expression was also similar for all three proteins. Background staining may be due to low levels of LCN2, HO-1, and F-LC released by cells. We suspect that these iron regulatory proteins may be actively secreted into the exterior of the cell in response to inflammation caused by alcohol presence (we have previously described the inflammatory footprints of alcohol in the CNS [25]). However, alcohol consumption dynamically changed iron management under TBI. LCN2 expression peaked at 24 hours in EtOH + FPI, same as that of FPI alone, but the presence of alcohol prolonged the expression of LCN2 for more than 7-days without altering the location or magnitude of FPI-induced LCN2 (**Fig. 2**, EtOH + FPI panels at 1-, 3-, and 7-days). The combined effects of EtOH + FPI was seen to induce HO-1 at 24 hours, earlier than with FPI alone (**Fig. 3**, EtOH + FPI panels at 1-, 3-, and 7-days). In addition, cellular expression density and intensity appeared greater than that of LCN2. Like FPI, EtOH + FPI-induced HO-1 presence was prominent at the hippocampus, neocortex, and around vessels near the site of impact. The notable combined effects of EtOH + FPI was impacted in the expression F-LC, wherein the increased levels of F-LC peaked at day 3 and sustained these levels up to 7-days (**Fig. 4**, EtOH + FPI panels at 1-, 3-, and 7-days).

*3.3 Activated microglia may also be involved in iron management.*

*3.3.1 Activation*

Sham injuries did not stimulate microglial activation and so microglia appeared resting with dynamic branching of their processes (**Fig. 6**, Sham panels at 1-, 3-, and 7-days). However, fully activated microglia in round ameboid shapes were observed as early as 1-day post-FPI. This morphology was sustained at 3-days but by 7-days post-FPI microglia returned to their homeostatic state (**Fig. 6**, FPI panels at 1-, 3-, and 7-days). In addition, the number of monocyte lineage cells, marked by CD68 expression, also significantly increased compared to sham controls ($p<0.001$) in plasma (**Fig. 5**).

Interestingly, we also observed a morphological gradient 3-days post-FPI. At the site of blood accumulation, the gathering microglia were in the active ameboid shape but, several micrometers away from this site resident microglia appeared stress-primed with short, thick processes. In this intermediary state, microglia are very reactive and can easily change to any other of the activation states. Microglia furthest away from bleed sites remained in a homeostatic, surveillance-inclined state (**Fig. 7.C**). Alcohol consumption alone resulted in sustained presence of activated microglia in and around the ventricular systems and inferior colliculus (**Fig. 6**, EtOH panels at 1-, 3-, and 7-days).

In FPI following chronic alcohol exposure, microglia also appeared activated at 1-day, invading cavities near the inferior colliculus. However, unlike in FPI or EtOH alone, there were greater numbers of microglia present. High microglial numbers were sustained 3-days post-EtOH + FPI, but by 7-days, with considerably less RBC presence, there were fewer of these immune cells. However, microglia sustained an activated form 1-, 3-, and 7-days under EtOH + FPI (**Fig. 6**, EtOH + FPI panels at 1-, 3-, and 7-days). Under alcohol alone, microglia remained activated for all days, therefore, the addition of FPI only reinforces continuation in this form. Interestingly, several of these microglia also appeared bigger in size. Further investigation revealed that microglia may be phagocytosing moribund RBCs.

### *3.3.2 Implied phagocytosis*

At 3-days post-FPI, sites with microglia and RBCs show these microglia ingesting individual, intact RBCs (**Fig. 7.A**). In that same area, a neighboring microglia cell, that has earlier phagocytosed an RBC, was found with free, ferrous iron inside its cell body (**Fig. 7.A**). The lack of surrounding free iron suggests that this cytoplasmic iron may come from the ingestion and breakdown of an RBC. However, microglia may also be phagocytosing iron-containing complexes seeing as bound, ferric iron was also found in microglia, otherwise, the iron released from ingested RBCs is quick sequestered as hemosiderin (**Fig. 7.B**). With FPI following chronic alcohol consumption at 1-day, microglia appeared more reactive, ingesting more than one RBC or iron-containing complex at a time, and increasing tremendously in size (**Fig. 7.B**). Conversely, the abundance of RBCs may simply force single microglia to ingest more. Phagocytosis was also implied under EtOH alone at sites with some RBC presence (**Fig. 6**, EtOH panels at 1-, 3-, and 7-days). Absence of CD68-positive staining confirm that these immune cells were not macrophage (not shown).

# 4. Discussion

*4.1 Excess iron in the CNS is regulated by three distinct pathways.*

*4.1.1 Hemosiderin and transferrin binding.*

Accumulation of red blood cells (RBCs) has been observed in fluid percussion injury (FPI) [32]. These RBCs come from blood vessels ruptured by the transient mechanical forces produced by the impact, in which hemorrhage lasts for several days resulting in substantial aggregations of RBCs especially in the epidural, subarachnoid, and ventricular spaces [33]. Failure to clear these RBC aggregates may cause the formation of an impacted blood mass and can result in an enduring mass effect. With time, RBC aggregates can penetrate neighboring tissue as we observed in our findings here (**Fig. 1**, Eosin + Prussian Blue at 2 hours and 7-days). This may be due to their low resistance and viscoelastic properties as have been previously noted by others [34]. Interestingly, the most penetration of RBCs was observed at subarachnoid spaces as opposed to any other area. Since the subarachnoid space facilitates fluid flow into the brain, RBCs may be using this current to enter brain tissue [35]. These RBCs homing in tissue cannot survive for a long time, lacking mitochondria and depleted of energy they eventually die and undergo hemolysis to release free irons. We found that iron remains ferrous for only a few hours following injury as ferric iron was observed as early as 1-day post-FPI (**Fig. 1**, Turnbull's Blue panel at 2 hours). This explanation is in agreement with the findings of others [22]. Free iron, whether as a ferrous cation or an unbound ferric species, is readily absorbed by cells and can be very toxic [36]. The unpaired electrons make free iron highly chemically reactive and, through the Fenton-Haber-Weiss reaction, catalyze the formation of free radicals. This may be a reason for iron's rapid transformation from ferrous to ferric, and finally to the bound form by the body.

Although transferrin increased following injury (**Fig. 5**), generally, transferrin becomes saturated when ~70% is bound with iron [37]. Western blot analysis showed greater F-LC levels in plasma than transferrin (**Fig. 5**). When this main iron binding protein in the blood is so far extended that it cannot bind any more iron, excess catalytic iron must be stored by ferritin or transformed ferritin, i.e., hemosiderin, to prevent iron toxicity. Significant amounts of hemosiderin collections, ranging in size, were found at all bleed sites (for example in **Fig. 7.B**). These results reveal hemosiderin binding as a pathway in iron management specially reserved for superfluous excesses of iron. Iron as hemosiderin is not readily available for release thereby making this binding very stable. We speculate that, like ferritin binding, iron release from hemosiderin may possibly be achieved by lysosomes. Extracellular hemosiderin complexes may also follow suit and be degraded by strong digestive enzymes. More research is needed on the fate of iron

following hemosiderin binding and on understanding the circumstances and elements involved in its release; it is likely lysosomes may be involved.

*4.1.2 Sequestration by iron regulatory proteins.*

Russell et. al. (2019) described a time-dependent induction of the iron regulatory proteins LCN2, HO-1, and F-LC following an FPI-induced traumatic brain injury [22]. They have also quantitatively shown significant increases in these proteins following FPI. We have observed similar results in rats that have undergone FPI alone but a time shift in expression profiles following prior alcohol consumption. In both FPI and EtOH + FPI situations we have observed a similar expression pattern for LCN2 (cartoon summary in **Fig. 8**). By immediately trafficking and sequestering iron, LCN2 expression stimulates anticipation for possible incoming or excess iron to prevent its congestion. This result demonstrates that LCN2 induction may not depend on the type of injury but rather by the inflammation associated with the injury. Therefore, if the injury causes any release of inflammatory stimuli, LCN2 becomes expressed. This result demonstrates that combined, alcohol and FPI injuries do not necessarily exacerbate the degree of inflammation, but rather prolong its persistence. However, failure to resolve this inflammation can lead to a chronic inflammatory state in the CNS and manifest debilitations in attention and cognition [38]. Therefore, by maintaining LCN2 expression, alcohol consumption may transform FPI-induced inflammatory properties. In this way, LCN2 may act as a master switch for the induction of subsequent iron regulatory proteins. LCN2 may occupy a greater role in iron regulation than has been so far suggested.

One important regulator of HO-1 expression is the nuclear transcription factor Nrf2 [39]. Nrf2 also controls production of the antioxidant proteins that protect against the oxidative damage caused by an insult. Therefore, HO-1 is directly related to the presence and extent of oxidative damage. We have previously shown that inflammation, from both FPI and the resulting hemorrhage, can trigger oxidative damage [12]. Since LCN2 expression is determined by inflammation and HO-1 is mediated by oxidative stress, HO-1 induction is expected to occur after LCN2 under FPI (**Fig. 8**). However, alcohol presence causes HO-1 to express concurrent with LCN2 (**Fig. 8**). EtOH + FPI must exacerbate oxidative damage enough to cause this shift to earlier protein expression.

Interestingly, F-LC was observed as clusters. F-LC clustering may be the result of a partial unfolding of the protein shell in preparation for iron binding [40]. Unlike ferritin heavy chain (F-HC), F-LC has no ferroxidase activity, instead it is involved in the transfer of electrons across its protein cage which allows F-LC staining to mark unfolded shells [41]. Notably, we observed a delayed ferritin response following FPI, peaking at 7-days (**Fig. 8**). These results demonstrate that ferritin is the final regulatory protein involved in iron management, sequestering any remaining unbound iron for accessible storage. Even hemosiderin, observed in 1-day post-FPI, precedes significant ferritin expression (**Fig. 4**, FPI panels at 1- and 3-days).

Furthermore, this delay shows ferritin to be induced primarily by iron release and secondarily by heme presence. Low ferritin levels under EtOH alone suggest that ferritin is nominally induced by stress. However, EtOH + FPI caused early, increased, and sustained ferritin expression. Due to the excess RBC accumulation following these combined injuries, much of this ferritin may be being excreted and transformed to hemosiderin for more stable storage. These increased ferritin levels also imply high iron concentrations in the CNS.

*4.1.3 IRPs also function in the extracellular space.*

Interestingly, LCN2, HO-1, and F-LC were also expressed directly atop bleed sites, interacting with RBCs. This presence may be explained by the mechanical forces caused by the impact bursting cells and releasing intracellular proteins into the extracellular space. As demonstrated, alcohol may also help facilitate secretion of these proteins by increasing their basal levels. There is evidence of LCN2, HO-1, and F-LC secretion in other organ systems. Hepatic cells have been shown to secrete ferritin, while HO-1 has been found in various extracellular, fluid filled compartments and LCN2, as a mediator of inflammation, is routinely released by various cell types, most notably immune cells [42-44]. Extrapolating these findings and relating then to the CNS space, HO-1 may be in the CSF while LCN2 gets secreted by astrocytes and microglia, and ferritin released by neurons. Then protein targeting mechanisms may explain their localization at sites of RBC aggregation. More research on the default expression levels and locations of LCN2, HO-1, and F-LC in the CNS as well as their intrinsic signaling sequences may help explain this phenomenon.

LCN2/HO-1 colocalization can indicate that even HO-1 may not be constrained to expression following FPI, instead it can be induced by the oxidative stress accompanying inflammation [45]. Meanwhile, LCN2/F-LC colocalization suggests LCN2 expression may recruit F-LC generation in preparation for iron sequestration. The lack of microglial expression of these iron regulatory proteins suggests microglia may not be involved in the lipocalin 2/heme oxygenase 1/ferritin system of iron management. Another limitation of this study was confining it to 7-days. However, previous studies have shown that beyond 7-days, LCN2, HO-1, and F-LC levels comparatively return, or begin to return, to basal levels in most cells of the CNS [22]. A notable exception are microglia which have shown elevated HO-1 expression as late as 30-days relative to controls under a moderate cortical impact [46]. In this effect, we argue that microglial involvement may create a separate pathway for iron management, removed from that created by the iron regulatory proteins of the remaining CNS cells.

*4.1.4 Implied microglial phagocytosis.*

Previous studies revealing iron presence in microglia have only considered its accumulation as iron retention and a signature of microglial activation [47]. The idea of a link between iron management, by extent metabolism, and activated microglia has been contemplated for some time [48]. Moreover, the capacity for RBC phagocytosis by microglial cells has already been well established as an important corrective response to CNS hemorrhage [49]. In agreement with previous studies, we have observed microglial activation following FPI alone in the present work, as well as following chronic alcohol exposure [50, 51]. Interestingly, many of these activated microglia remained in the tissue at 1-day, only being present around RBCs and bleed sites 3-days post-FPI. These results demonstrate that morphology precedes function and, although reacting quickly to an injury, microglia may have a delayed immune response to invading RBCs. However, microglia may be responding to only atypical RBCs such as those dying from nutrient deprivation after being confined in tissue for 3-days post-FPI.

Other studies as well as our own also observed ethanol induced microglial activation [24, 52-54]. Expectedly, the combination likewise caused microglia activation and greater numbers to gather at sites with RBC aggregation (**Fig. 7.B**). Chronic alcohol use prior to FPI may be sensitizing microglia to stress and, in this manner, preconditioning the brain to future injuries. In other words, the CNS stays in 'high alert' for possible stress so that when stress does appear an appropriate response is rapidly mobilized. This state of hypervigilance may dysregulate inflammatory and immune responses to cause inappropriate and even exaggerated reactions. In this respect we observed multiple RBCs within activated microglia following EtOH + FPI. This excessive ingestion may either be due to chronic phagocytic activity or the engulfment of multiple RBCs at once. Similarly, the increased number of microglia present may either be the result of migration, division, or a degree of both. One limitation of this study is the lack of follow-up staining for cell surface markers upregulated by microglial phagocytosis, therefore, this observed microglial ingestion can only imply phagocytosis. Our future work will include studies exploring these fundamental possibilities. A recent study has shown that microglia can assume a range of phenotypes under alcohol dependency and much remains to be understood in regard to their activation [55].

Collectively, these results begin to postulate a distinct pathway for iron maintenance by microglial cells (**Fig. 9**). Activated microglia may phagocytose and hemolyze RBCs, catabolize heme, and release free iron. Immediately, this iron may get bound to ferritin or hemosiderin. Any extracellular free iron then becomes bound to apotransferrin or hemosiderin to form iron-containing complexes. Knowledge of macrophage iron management can be used to infer other details of the microglial-centric pathway. One role of macrophage is to phagocytosis of senescent RBCs [56]. Therefore, in behaving like macrophage, activated microglia may also phagocytose RBC aggregations and, in so doing, regulate excess iron presence in the CNS. Heme transporters may also be involved in transporting heme into the cell or release it from plasma membrane-derived vacuoles following phagocytosis. Increases in the labile iron pool may cause excess iron to catalyze production of reactive oxygen species. Iron release may be inhibited by hepcidin hormone binding to and degrading ferroportin transporters. As iron can only bind when in the ferric form, membrane bound ferroxidases may be oxidizing the ferrous form. As an additional idea, the debris following RBC hemolysis and heme release may be shuffled to lysosomes for degradation. Any

lysosomal iron may be combined with partially degraded ferritin protein to create hemosiderin. Finally, additional stressors may free iron and evoke toxicity such as ferroptosis, an iron-dependent programmed cell death [57]. Many directions remain to be studied in an effort to understand iron management by microglial cells. We have only begun to discover this alternative pathway of iron regulation.

*4.2 Alcohol's influence extends to iron management.*

Being soluble in water, alcohol distributes into fluid spaces, as a result, higher concentrations of ethanol can be found in blood, or cerebral spinal fluid (CSF) surround the brain [58]. As the major alcohol filtrating and metabolizing organ of the body, the liver becomes an obvious site for alcohol-induced iron build-up [59]. In fact, this iron accumulation has been shown to contribute to the onset of alcoholic liver disease. This then develops into hepatitis and, over time, liver cirrhosis and destruction. In these same respects, generation of iron deposits in the brain may also lead to a form of inflammation and, if not corrected, neurodegeneration. We have shown that alcohol consumption increases bleeding and consequent iron deposition in the CNS (**Fig. 7.B**). In addition, alcohol abuse has also been shown to frequent rebleeding incidents and, in so doing, can augment deposition numbers even more so [60]. Despite this, we did not observe noticeable amounts of ferrous iron under EtOH + FPI. Therefore, although alcohol consumption significantly increases iron load in the CNS, the iron regulatory mechanisms adapt to accommodate this upsurge and prevent free iron accumulation and iron toxicity. To this effect, we have shown that prior chronic alcohol exposure changes the response of all three iron management pathways following FPI (cartoon summary in **Fig. 8**). It may be that continued chronic alcohol consumption following FPI is required to release hemosiderin bound iron. This persistent stress would prevent inflammation from resolving and deregulate CNS functions. One affected system may be iron storage wherein the hemosiderin protein complex becomes destabilized and releases iron. Our future research will examine iron aggregation and regulation when chronic alcohol consumption is continued following FPI (an EtOH + FPI + ETOH model).

# 5. Conclusion

The iron management system in the body is very efficient, especially so in the CNS. Three distinct pathways coordinate to ensure iron is only ever briefly unbound. The LCN2/HO-1/F-LC arrangement serves to identify, extract, and sort excess iron coming from its primary source, hemorrhage. Meanwhile, transferrin and hemosiderin binding control the overflow. We have shown that microglia may play a role as well in clearing away some RBCs and iron deposits. However, as a secondary stressor, alcohol exposure increases hemorrhage and RBC accumulation following FPI. This results in alterations to the expression patterns of the iron regulatory proteins LCN2, HO-1, and F-LC. In addition, alcohol increases recruitment and activation of possibly phagocytosing microglia. In effect, prior alcohol abuse

exacerbates iron accumulation following a traumatic brain injury and alters the iron management system in the CNS.

# Declarations

### Ethics Approval

Not applicable

### Consent to participate

Not applicable

### Consent for publication

Not applicable

### Availability of data and materials

The datasets generated during and/or analyzed during the current study are available from the corresponding author on reasonable request.

### Competing interests

The authors declare that they have no competing interests.


### Funding

This work was supported by a grant from the NIH/NIAAA (#5R21AA028340-02) awarded to JH.


### Authors' contributions

AA carried out the studies, acquired the data, and was involved with preparing the manuscript. AR acquired the images and helped AA analyze data. XM and YC conducted the alcohol feeding and performed the fluid percussion injury. KB proofread the manuscript and provided important comments.

JH design the project and was involved with preparing the manuscript. All authors read and approved the final manuscript.


### Acknowledgments

This work was supported by a grant from the NIH/NIAAA (#5R21AA028340-02) awarded to JH.


### Authors' statement

All authors certify that they have participated sufficiently in the work to take responsibility for the content. Each author certifies that this material has not been previously published or submitted for publication elsewhere. This work has been posted as a pre-print with Research Square
DOI: https://doi.org/10.21203/rs.3.rs-991124/v1. This work is licensed under a CC BY 4.0 License. [61]

### Compliance with Ethical Standards

### Disclosure of potential conflicts of interest

The authors declare that they have no potential conflicts of interest.

### Research involving Human Participants and/or Animals

All experiments were conducted in accordance with the National Institutes of Health institutional ethical guidelines for care of laboratory animals and approved by the Institutional Animal Care Use Committee of Rutgers University (Newark, NJ), IACUC Protocol No. PROTO999900801.

### Informed Consent

Not applicable

## References


1. Aravind, A., A.R. Ravula, N. Chandra, and B.J. Pfister, *Behavioral Deficits in Animal Models of Blast Traumatic Brain Injury.* Frontiers in Neurology, 2020. **11**(990).

2. Kuriakose, M., D. Younger, A.R. Ravula, E. Alay, K.V. Rama Rao, and N. Chandra, *Synergistic Role of Oxidative Stress and Blood-Brain Barrier Permeability as Injury Mechanisms in the Acute Pathophysiology of Blast-induced Neurotrauma.* Sci Rep, 2019. **9**(1): p. 7717.

3. Nyanzu, M., F. Siaw-Debrah, H. Ni, Z. Xu, H. Wang, X. Lin, Q. Zhuge, and L. Huang, *Improving on Laboratory Traumatic Brain Injury Models to Achieve Better Results.* Int J Med Sci, 2017. **14**(5): p. 494-505.

4. Rana, P., K.V. Rama Rao, A. Ravula, R. Trivedi, M. D'Souza, A.K. Singh, R.K. Gupta, and N. Chandra, *Oxidative stress contributes to cerebral metabolomic profile changes in animal model of blast-induced traumatic brain injury.* Metabolomics, 2020. **16**(3): p. 39.

5. Lee, J.J., D.J. Segar, J.F. Morrison, W.M. Mangham, S. Lee, and W.F. Asaad, *Subdural hematoma as a major determinant of short-term outcomes in traumatic brain injury.* J Neurosurg, 2018. **128**(1): p. 236-249.

6. Perel, P., I. Roberts, O. Bouamra, M. Woodford, J. Mooney, and F. Lecky, *Intracranial bleeding in patients with traumatic brain injury: A prognostic study.* BMC Emergency Medicine, 2009. **9**(1): p. 15.

7. Schweitzer, A.D., S.N. Niogi, C.T. Whitlow, and A.J. Tsiouris, *Traumatic Brain Injury: Imaging Patterns and Complications.* RadioGraphics, 2019. **39**(6): p. 1571-1595.

8. Weil, Z.M., J.D. Corrigan, and K. Karelina, *Alcohol Use Disorder and Traumatic Brain Injury.* Alcohol Res, 2018. **39**(2): p. 171-180.

9. Teng SX, M.P., *Acute Alcohol Intoxication Prolongs Neuroinflammation without Exacerbating Neurobehavioral Dysfunction following Mild Traumatic Brain Injury.* Journal of Neurotrauma, 2014. **31**(4): p. 378-386.

10. Lowe, P.P., C. Morel, A. Ambade, A. Iracheta-Vellve, E. Kwiatkowski, A. Satishchandran, I. Furi, Y. Cho, B. Gyongyosi, D. Catalano, E. Lefebvre, L. Fischer, S. Seyedkazemi, D.P. Schafer, and G. Szabo, *Chronic alcohol-induced neuroinflammation involves CCR2/5-dependent peripheral macrophage infiltration and microglia alterations.* J Neuroinflammation, 2020. **17**(1): p. 296.

11. Smith, S., K. Fair, A. Goodman, J. Watson, C. Dodgion, and M. Schreiber, *Consumption of alcohol leads to platelet inhibition in men.* The American Journal of Surgery, 2019. **217**(5): p. 868-872.

12. Ma, X., Y. Cheng, R. Garcia, and J. Haorah, *Hemorrhage Associated Mechanisms of Neuroinflammation in Experimental Traumatic Brain Injury.* J Neuroimmune Pharmacol, 2020. **15**(2): p. 181-195.

13. Ma, X., A. Aravind, B.J. Pfister, N. Chandra, and J. Haorah, *Animal Models of Traumatic Brain Injury and Assessment of Injury Severity.* Mol Neurobiol, 2019. **56**(8): p. 5332-5345.

14. East, J.M., J. Viau-Lapointe, and V.A. McCredie, *Transfusion practices in traumatic brain injury.* Curr Opin Anaesthesiol, 2018. **31**(2): p. 219-226.

15. Stolla, M., F. Zhang, M.R. Meyer, J. Zhang, and J.-F. Dong, *Current state of transfusion in traumatic brain injury and associated coagulopathy.* Transfusion, 2019. **59**(S2): p. 1522-1528.

16. Salim, A., P. Hadjizacharia, J. DuBose, C. Brown, K. Inaba, L. Chan, and D.R. Margulies, *Role of anemia in traumatic brain injury.* J Am Coll Surg, 2008. **207**(3): p. 398-406.

17. Daglas, M. and P.A. Adlard, *The Involvement of Iron in Traumatic Brain Injury and Neurodegenerative Disease.* Front Neurosci, 2018. **12**: p. 981.

18. Magnani, M., V. Stocchi, L. Cucchiarini, L. Chiarantini, and G. Fornaini, *Red blood cell phagocytosis and lysis following oxidative damage by phenylhydrazine.* Cell Biochem Funct, 1986. **4**(4): p. 263-9.

19. Wimmer, I., C. Scharler, T. Kadowaki, S. Hillebrand, B. Scheiber-Mojdehkar, S. Ueda, M. Bradl, T. Berger, H. Lassmann, and S. Hametner, *Iron accumulation in the choroid plexus, ependymal cells and CNS parenchyma in a rat strain with low-grade haemolysis of fragile macrocytic red blood cells.* Brain Pathol, 2021. **31**(2): p. 333-345.

20. Izatt, R.M., G.D. Watt, C.H. Bartholomew, and J.J. Christensen, *Calorimetric study of Prussian blue and Turnbull's blue formation.* Inorganic Chemistry, 1970. **9**(9): p. 2019-2021.

21. Dev, S. and J.L. Babitt, *Overview of iron metabolism in health and disease.* Hemodialysis International, 2017. **21**(S1): p. S6-S20.

22. Russell, N.H., R.T. Black, N.N. Lee, A.E. Doperalski, T.M. Reeves, and L.L. Phillips, *Time-dependent hemeoxygenase-1, lipocalin-2 and ferritin induction after non-contusion traumatic brain injury.* Brain Research, 2019. **1725**: p. 146466.

23. Donat, C.K., G. Scott, S.M. Gentleman, and M. Sastre, *Microglial Activation in Traumatic Brain Injury.* Frontiers in Aging Neuroscience, 2017. **9**(208).

24. Murugan, M., A. Ravula, A. Gandhi, G. Vegunta, S. Mukkamalla, W. Mujib, and N. Chandra, *Chemokine signaling mediated monocyte infiltration affects anxiety-like behavior following blast injury.* Brain, Behavior, and Immunity, 2020. **88**: p. 340-352.

25. Alikunju, S., P.M. Abdul Muneer, Y. Zhang, A.M. Szlachetka, and J. Haorah, *The inflammatory footprints of alcohol-induced oxidative damage in neurovascular components.* Brain, Behavior, and Immunity, 2011. **25**: p. S129-S136.

26. Cheng, Y., X. Ma, K.D. Belfield, and J. Haorah, *Biphasic Effects of Ethanol Exposure on Waste Metabolites Clearance in the CNS.* Molecular Neurobiology, 2021.

27. Muneer, P.M.A., S. Alikunju, A.M. Szlachetka, and J. Haorah, *The Mechanisms of Cerebral Vascular Dysfunction and Neuroinflammation by MMP-Mediated Degradation of VEGFR-2 in Alcohol Ingestion.* Arteriosclerosis, Thrombosis, and Vascular Biology, 2012. **32**(5): p. 1167-1177.

28. Sarkar, B., X. Ma, A. Agas, Z. Siddiqui, P. Iglesias-Montoro, P.K. Nguyen, K.K. Kim, J. Haorah, and V.A. Kumar, *In vivo neuroprotective effect of a self-assembled peptide hydrogel.* Chemical Engineering Journal, 2021. **408**: p. 127295.

29. Blomster, L.V., G.J. Cowin, N.D. Kurniawan, and M.J. Ruitenberg, *Detection of endogenous iron deposits in the injured mouse spinal cord through high-resolution ex vivo and in vivo MRI.* NMR Biomed, 2013. **26**(2): p. 141-50.

30. Crowe, A., W. Zheng, J. Miller, S. Pahwa, K. Alam, K.-M. Fung, E. Rubin, F. Yin, K. Ding, and W. Yue, *Characterization of Plasma Membrane Localization and Phosphorylation Status of Organic Anion Transporting Polypeptide (OATP) 1B1 c.521 T>C Nonsynonymous Single-Nucleotide Polymorphism.* Pharmaceutical research, 2019. **36**(7): p. 101-101.

31. Crowe, A.R. and W. Yue, *Semi-quantitative Determination of Protein Expression using Immunohistochemistry Staining and Analysis: An Integrated Protocol.* Bio-protocol, 2019. **9**(24): p. e3465.

32. Dietrich, W.D., O. Alonso, R. Busto, R. Prado, S. Dewanjee, M.K. Dewanjee, and M.D. Ginsberg, *Widespread hemodynamic depression and focal platelet accumulation after fluid percussion brain injury: a double-label autoradiographic study in rats.* J Cereb Blood Flow Metab, 1996. **16**(3): p. 481-9.

33. McKee, A.C. and D.H. Daneshvar, *The neuropathology of traumatic brain injury.* Handbook of clinical neurology, 2015. **127**: p. 45-66.

34. Weisel, J.W. and R.I. Litvinov, *Red blood cells: the forgotten player in hemostasis and thrombosis.* Journal of Thrombosis and Haemostasis, 2019. **17**(2): p. 271-282.

35. Cheng, Y. and J. Haorah, *How does the brain remove its waste metabolites from within?* Int J Physiol Pathophysiol Pharmacol, 2019. **11**(6): p. 238-249.

36. Imai, T., S. Iwata, T. Hirayama, H. Nagasawa, S. Nakamura, M. Shimazawa, and H. Hara, *Intracellular Fe(2+) accumulation in endothelial cells and pericytes induces blood-brain barrier dysfunction in secondary brain injury after brain hemorrhage.* Sci Rep, 2019. **9**(1): p. 6228.

37. Eid, R., N.T. Arab, and M.T. Greenwood, *Iron mediated toxicity and programmed cell death: A review and a re-examination of existing paradigms.* Biochim Biophys Acta Mol Cell Res, 2017. **1864**(2): p. 399-430.

38. Balter, L.J.T., J.A. Bosch, S. Aldred, M.T. Drayson, J.J.C.S. Veldhuijzen van Zanten, S. Higgs, J.E. Raymond, and A. Mazaheri, *Selective effects of acute low-grade inflammation on human visual attention.* NeuroImage, 2019. **202**: p. 116098.

39. Kim, K.W., C.S. Yoon, Y.C. Kim, and H. Oh, *Desoxo-narchinol A and Narchinol B Isolated from Nardostachys jatamansi Exert Anti-neuroinflammatory Effects by Up-regulating of Nuclear Transcription Factor Erythroid-2-Related Factor 2/Heme Oxygenase-1 Signaling.* Neurotox Res, 2019. **35**(1): p. 230-243.

40. Shin, M.K., S.I. Kim, S.J. Kim, S.Y. Park, Y.H. Hyun, Y. Lee, K.E. Lee, S.S. Han, D.P. Jang, Y.B. Kim, Z.H. Cho, I. So, and G.M. Spinks, *Controlled magnetic nanofiber hydrogels by clustering ferritin.* Langmuir, 2008. **24**(21): p. 12107-11.

41. Arosio, P., L. Elia, and M. Poli, *Ferritin, cellular iron storage and regulation.* IUBMB Life, 2017. **69**(6): p. 414-422.

42. Li Volti, G., F. Galvano, A. Frigiola, S. Guccione, C. Di Giacomo, S. Forte, G. Tringali, M. Caruso, O.A. Adekoya, and D. Gazzolo, *Potential immunoregulatory role of heme oxygenase-1 in human milk: a combined biochemical and molecular modeling approach.* J Nutr Biochem, 2010. **21**(9): p. 865-71.

43. Moschen, A.R., T.E. Adolph, R.R. Gerner, V. Wieser, and H. Tilg, *Lipocalin-2: A Master Mediator of Intestinal and Metabolic Inflammation.* Trends Endocrinol Metab, 2017. **28**(5): p. 388-397.

44. Tran, T.N., S.K. Eubanks, K.J. Schaffer, C.Y.J. Zhou, and M.C. Linder, *Secretion of Ferritin by Rat Hepatoma Cells and Its Regulation by Inflammatory Cytokines and Iron.* Blood, 1997. **90**(12): p. 4979-4986.

45. Jin, Z., K.E. Kim, H.J. Shin, E.A. Jeong, K.A. Park, J.Y. Lee, H.S. An, E.B. Choi, J.H. Jeong, W. Kwak, and G.S. Roh, *Hippocampal Lipocalin 2 Is Associated With Neuroinflammation and Iron-Related Oxidative Stress in ob/ob Mice.* J Neuropathol Exp Neurol, 2020. **79**(5): p. 530-541.

46. Morita, A., A. Jullienne, A. Salehi, M. Hamer, E. Javadi, Y. Alsarraj, J. Tang, J.H. Zhang, W.J. Pearce, and A. Obenaus, *Temporal evolution of heme oxygenase-1 expression in reactive astrocytes and microglia in response to traumatic brain injury.* Brain Hemorrhages, 2020. **1**(1): p. 65-74.

47. McIntosh, A., V. Mela, C. Harty, A.M. Minogue, D.A. Costello, C. Kerskens, and M.A. Lynch, *Iron accumulation in microglia triggers a cascade of events that leads to altered metabolism and compromised function in APP/PS1 mice.* Brain Pathol, 2019. **29**(5): p. 606-621.

48. Mairuae, N., J.R. Connor, and P. Cheepsunthorn, *Increased cellular iron levels affect matrix metalloproteinase expression and phagocytosis in activated microglia.* Neurosci Lett, 2011. **500**(1): p. 36-40.

49. Lan, X., X. Han, Q. Li, Q.W. Yang, and J. Wang, *Modulators of microglial activation and polarization after intracerebral haemorrhage.* Nat Rev Neurol, 2017. **13**(7): p. 420-433.

50. Loane, D.J. and A. Kumar, *Microglia in the TBI brain: The good, the bad, and the dysregulated.* Experimental Neurology, 2016. **275**: p. 316-327.

51. Walter, T.J., R.P. Vetreno, and F.T. Crews, *Alcohol and Stress Activation of Microglia and Neurons: Brain Regional Effects.* Alcohol Clin Exp Res, 2017. **41**(12): p. 2066-2081.

52. Fernandez-Lizarbe, S., M. Pascual, and C. Guerri, *Critical Role of TLR4 Response in the Activation of Microglia Induced by Ethanol.* The Journal of Immunology, 2009. **183**(7): p. 4733-4744.

53. Mishra, V., A. Agas, H. Schuetz, J. Kalluru, and J. Haorah, *Alcohol induces programmed death receptor-1 and programmed death-ligand-1 differentially in neuroimmune cells.* Alcohol, 2020. **86**: p. 65-74.

54. Zhao, Y.-N., F. Wang, Y.-X. Fan, G.-F. Ping, J.-Y. Yang, and C.-F. Wu, *Activated microglia are implicated in cognitive deficits, neuronal death, and successful recovery following intermittent ethanol exposure.* Behavioural Brain Research, 2013. **236**: p. 270-282.

55. Peng, H. and K. Nixon, *Microglia Phenotypes Following the Induction of Alcohol Dependence in Adolescent Rats.* Alcohol Clin Exp Res, 2021. **45**(1): p. 105-116.

56. Klei, T.R., S.M. Meinderts, T.K. van den Berg, and R. van Bruggen, *From the Cradle to the Grave: The Role of Macrophages in Erythropoiesis and Erythrophagocytosis.* Front Immunol, 2017. **8**: p. 73.

57. Li, J., F. Cao, H.L. Yin, Z.J. Huang, Z.T. Lin, N. Mao, B. Sun, and G. Wang, *Ferroptosis: past, present and future.* Cell Death Dis, 2020. **11**(2): p. 88.

58. Abrahao, K.P., A.G. Salinas, and D.M. Lovinger, *Alcohol and the Brain: Neuronal Molecular Targets, Synapses, and Circuits.* Neuron, 2017. **96**(6): p. 1223-1238.

59. Ioannou, G.N., J.A. Dominitz, N.S. Weiss, P.J. Heagerty, and K.V. Kowdley, *The effect of alcohol consumption on the prevalence of iron overload, iron deficiency, and iron deficiency anemia.* Gastroenterology, 2004. **126**(5): p. 1293-301.

60. Kärkkäinen, J.M., S. Miilunpohja, T. Rantanen, J.M. Koskela, J. Jyrkkä, J. Hartikainen, and H. Paajanen, *Alcohol Abuse Increases Rebleeding Risk and Mortality in Patients with Non-variceal Upper Gastrointestinal Bleeding.* Dig Dis Sci, 2015. **60**(12): p. 3707-15.

61. Agnieszka, A., R. Arun Reddy, M. Xiaotang, C. Yiming, D.B. Kevin, and H. James, Research Square, 2022.

# Tables

Table 1 is in the supplementary files section.

# Figures


**Figure 1**

Ferrous and ferric iron expression following FPI. The left and middle column are representative images of presence of both ferrous ($Fe^{+2}$) and ferric ($Fe^{+3}$) iron at sham injury (Sham), and 2 hrs and 7-days following moderate fluid percussion injury. Turnbull's blue method stains for free or ferrous iron while Prussian blue stains for ferric iron bound as hemosiderin. Both ferrous and ferric iron are stained blue while blood is distinguished by the yellow-brown bilirubin pigment. The right column are representative images of red blood cell penetration into the tissue over time. The yellow arrow points to an accumulation of red blood cells. Red blood cells are stained dark pink, iron is blue, and tissue is light pink. All images are focused near the ventricular systems or subarachnoid spaces, sites for major blood accumulation post-injury. The black bar represents 100 μm.

**Figure 2**

LCN2 induction by alcohol, FPI, and the combination. Representative images of lipocalin 2 expression in rats under sham injury (Sham), ethanol feeding (EtOH), fluid percussion injury (FPI), and injury following ethanol feeding (EtOH + FPI) 1-, 3-, and 7-days post-injury. Images focus on the neocortex at the site of impact. LCN2 is stained brown, nuclei purple, and positive ferric iron staining appears as black. The yellow arrows point to LCN2 expression around both longitudinal and cross-section vessels. The insets are higher magnifications of cells within the black box and demonstrate LCN2 generation by a single cell. The black bar represents 100 μm and inset bar represents 25 μm. Bar graph is a semi-quantitative analysis of LCN2 expression from the images. Results are presented as mean values (±SD, N = 4 rats). Significant difference is indicated by $* p \leq 0.05$ and $** p \leq 0.01$.


## Figure 3

HO-1 induction by alcohol, FPI, and the combination. Representative images of heme oxygenase 1 expression in rats under sham injury (Sham), ethanol feeding (EtOH), fluid percussion injury (FPI), and injury following ethanol feeding (EtOH + FPI) 1-, 3-, and 7-days post-injury. Images focus on the neocortex at the site of impact. HO-1 is stained brown and positive ferric iron staining appears as black. Sham sections also stain for vessels as red. The yellow arrows point to HO-1 expression around both

longitudinal and cross-section vessels. The insets are higher magnifications of cells within the black box and demonstrate HO-1 generation by a single cell. The black bar represents 100 μm and inset bar represents 25 μm. Bar graph is a semi-quantitative analysis of HO-1 expression from the images. Results are presented as mean values (N = 4 rats). Significant difference is indicated by ∗ p ≤ 0.05 and ∗∗ p ≤ 0.01.

## Figure 4

F-LC induction by alcohol, FPI, and the combination. Representative images of ferritin light chain expression in rats under sham injury (Sham), ethanol feeding (EtOH), fluid percussion injury (FPI), and injury following ethanol feeding (EtOH + FPI) 1-, 3-, and 7-days post-injury. Images focus on the hypothalamic and basal forebrain regions. F-LC is stained brown, red blood cells/vessels are red, ferric iron is dark navy, and tissue is light pink. The yellow arrows point to a cluster of F-LC expression. The inset is a higher magnification of cells within the black box and demonstrates F-LC generation at sites of red blood cell and iron accumulation. The black bar represents 100 μm and inset bar represents 25 μm. Bar graph is a semi-quantitative analysis of F-LC expression from the images. Results are presented as mean values (N = 4 rats). Significant difference is indicated by ∗ p ≤ 0.05, ∗∗ p ≤ 0.01, and ∗∗∗ p ≤ 0.001.

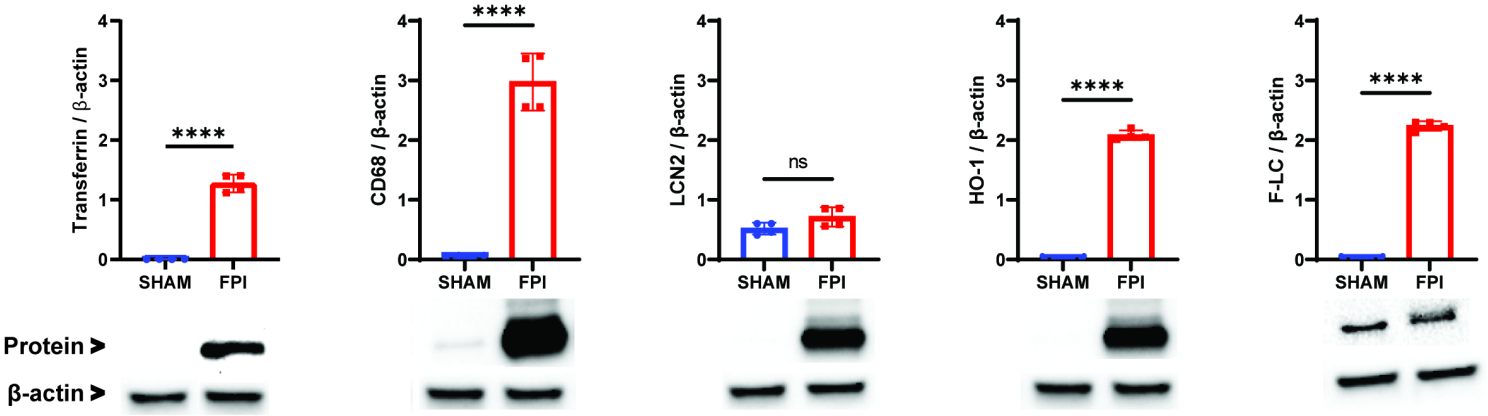


## Figure 5

Bar graphs showing western blot analysis of transferrin (TF), monocyte/macrophage marker (CD68), ferritin light chain (FTL), heme oxygenase 1 (HO-1), and lipocalin 2 (LCN2) levels in whole body blood plasma following sham and FPI injuries. Data were analyzed using ImageJ to obtain arbitrary densitometry intensities and quantified as the ratio of iron regulatory protein (IRP) to β-actin. Quantification was done on the original bands while the blots in the figure are cleaned representations. Results are presented as mean values (±SD, N = 4 rats). FPI is compared to Sham injury for each protein. Significant difference is indicated by ∗∗∗∗ p ≤ 0.001, n.s. denotes no significance.

## Figure 6

Microglial recruitment and activation by alcohol, FPI, and the combination. Representative images of the microglia-specific calcium-binding protein, Iba1, expression in rats under sham injury (Sham), ethanol feeding (EtOH), fluid percussion injury (FPI), and injury following ethanol feeding (EtOH + FPI) 1-, 3-, and 7-days post-injury. Sham images focus on the neocortex at the site of impact while EtOH, FPI, and EtOH + FPI images are focused near the ventricular systems and inferior colliculus at sites with major blood accumulation. Microglia are stained brown, cell nuclei are blue, red blood cells/vessels are red, ferric iron is purple, and tissue is light pink. The yellow arrows point to microglial recruitment to ventricular cavities and sites of red blood cell accumulation. The insets are higher magnifications of cells within the black box and demonstrate changes in microglial morphology following injury. Homeostatic, resting microglia exhibit dynamic branching while activated microglia take on an amoeboid form. Microglia in transition to the ameboid form have shortener, thicker processes. The black bar represents 100 μm and inset bar represents 25 μm. Bar graph shows percentage of amoeboid microglia (indicated by morphology and Iba1 staining) relative to cell count near the ventricular systems and inferior colliculus at sites with major blood accumulation (N = 4 rats). Significant difference is indicated by ∗∗ $p \leq 0.01$ and ∗∗∗∗ $p \leq 0.0001$.

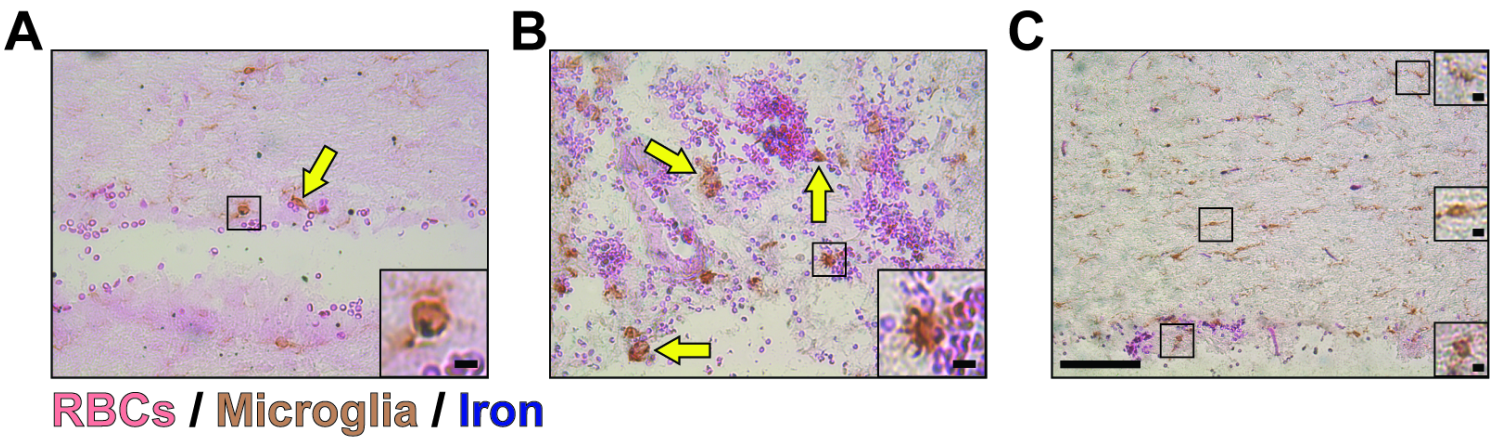


## Figure 7

Microglial phagocytosis of accumulated red blood cells. (A) Representative image of possible microglial phagocytosis of red blood cells near the ventricular systems 3-days post-FPI. The iron stained is in the free, ferrous form. (B) Representative image of possible microglial phagocytosis of red blood cells in the cavities next to the inferior colliculus 1-day post-EtOH + FPI. The iron stained is in the bound, ferric form. (C) Representative image of a morphological gradient 3-days post-FPI. Microglia next to red blood cells have an ameboid form, those near bleed sites are primed with shorter, thicker processes, and microglia even further away remain in a resting, ramified state. For all images, microglia are stained brown, iron is blue, red blood cells are dark pink, and tissue is light pink. The yellow arrows point to active or possible completed phagocytosis. The insets are higher magnifications of cells within the black box and demonstrate (A and B) presence of iron and red blood cells inside the microglia or (C) changes in

microglial morphology near bleed sites. The black bar represents 100 μm and inset bar represents 25 μm (A and B) and 12.5 μm (C).

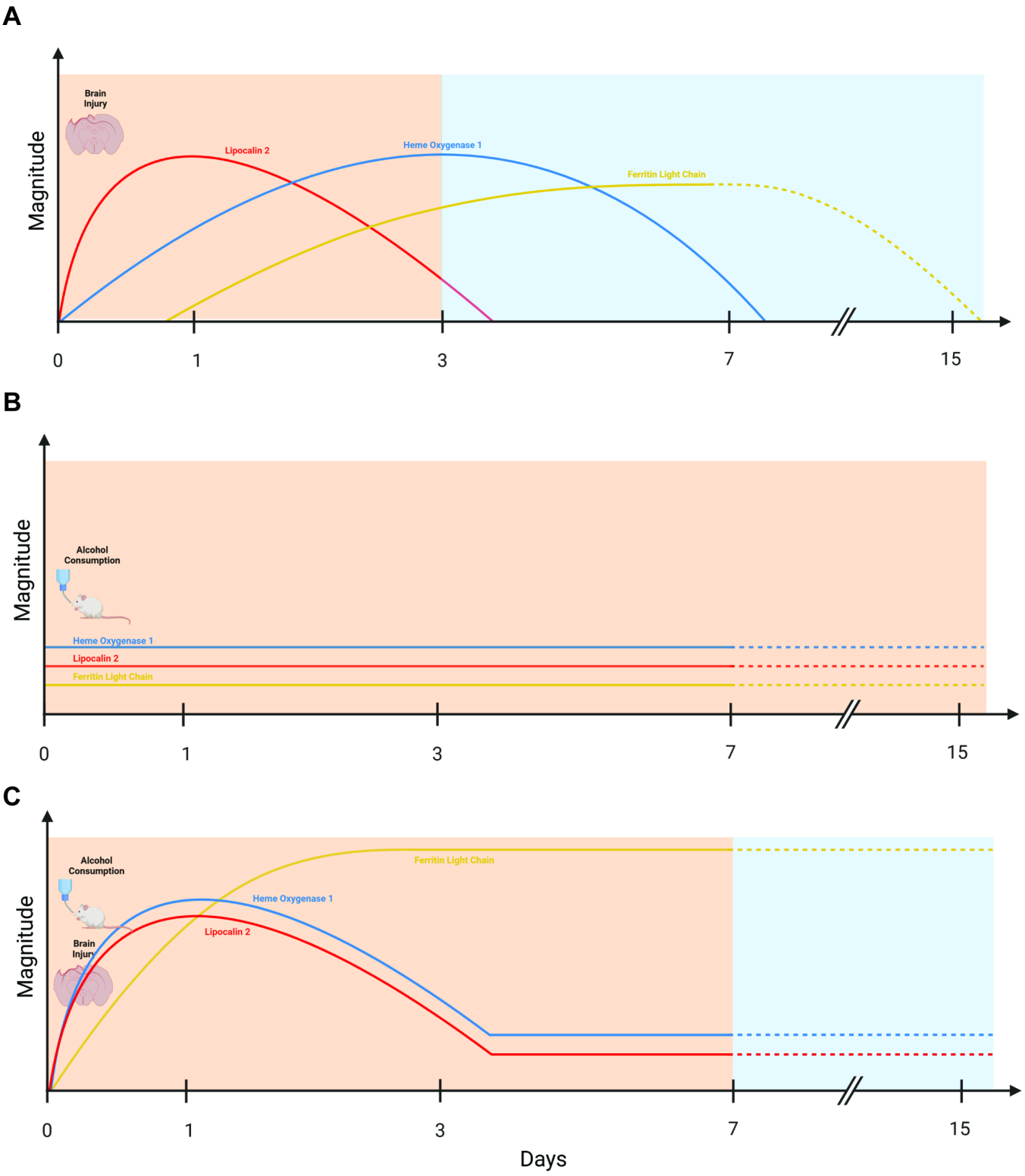


## Figure 8

Summary of LCN2, HO-1, and F-LC presence over time. Cartoon graphs depict a representative expression length and magnitude of each iron regulatory protein after its induction by (A) brain injury, (B) alcohol

consumption, or (C) the combination. The magnitude units are arbitrary, time is expressed in days with Day 0 representing injury initiation. The red, blue, and yellow lines denote LNC2, HO-1, and F-LC respectfully. The dashed lines speculate expression after 7-days post-injury. The light orange shading signifies hemorrhage/a pro-inflammatory response while the light blue shading signifies repair/an anti-inflammatory response. All cartoons were created with BioRender.com.

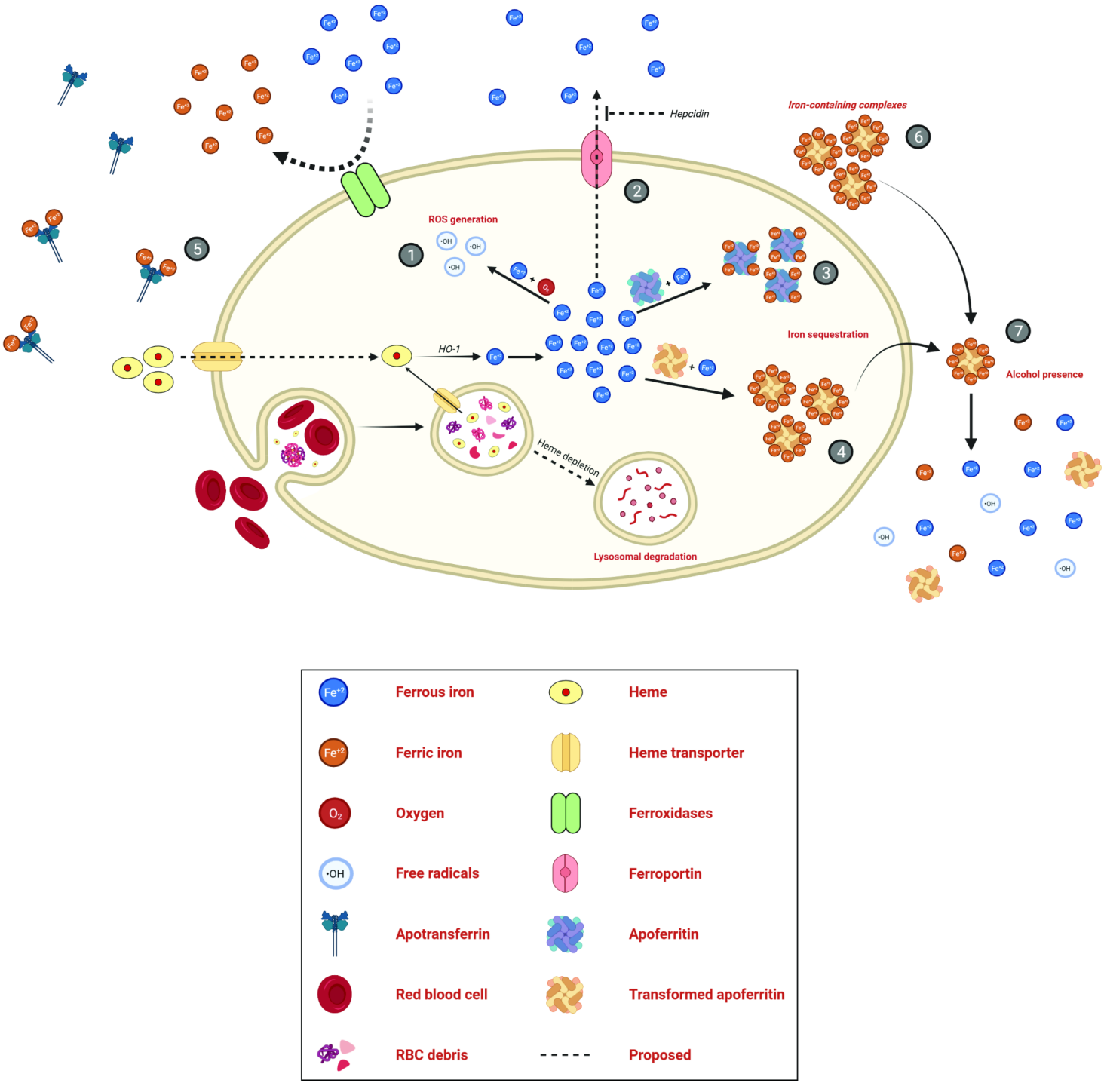


**Figure 9**

Schematic of iron regulation by activated microglia. Cartoon depicts pathways for microglial management of excess iron following traumatic brain injury. Activated microglia possibly phagocytose red blood cells whereupon heme becomes released. Following heme depletion, any remaining debris may be transported to lysosomes for degradation. Alternatively, extracellular heme may be transferred into the microglia via a heme transporter. Cytosolic heme can be lysed by heme oxygenase 1 to release free iron and increase the labile iron pool. Excessive intracellular iron can be: (1) oxidized to produce reactive oxygen species, (2) released by ferroportin transporters, (3) stored by ferritin, or (4) bound as hemosiderin for long term storage. Excessive extracellular iron can be converted to the more stable, ferric form by ferroxidases and (5) bind to apotransferrin for transportation or, when apotransferin becomes saturated, (6) be stored in iron-containing vesicles. (7) However, in the presence of alcohol, stored iron may be released, converted to its toxic, ferrous form by ferrireductase, and, as a result, generate oxidative stress. The pink text indicates a representative image that depicts this event. The cartoon was created with BioRender.com.

## Supplementary Files

This is a list of supplementary files associated with this preprint. Click to download.

- GraphicalAbstract.tif
- Table.tif